28 May 1999

ELSEVIER

Chemical Physics Letters 305 (1999) 319–326

CHEMICAL PHYSICS LETTERS

State and energy characterisation of fluorine atoms in the A band photodissociation of F_2

Melanie Roth [a], Christof Maul [a], Karl-Heinz Gericke [a,*], Takehito Senga [b], Masahiro Kawasaki [b]

[a] *Institut für Physikalische und Theoretische Chemie, Technische Universität Braunschweig, Hans-Sommer-Strasse 10, D-38106 Braunschweig, Germany*

[b] *Department of Molecular Engineering, Kyoto University, Kyoto 606-8501, Japan*

Received 15 March 1999; in final form 29 March 1999

Abstract

The fluorine photodissociation dynamics in the first absorption band was completely characterised by detection of atomic fluorine using resonantly enhanced multi-photon ionisation (REMPI). Jet-cooled parent molecules were excited into the repulsive $A^1\Pi_u$ state by a $3\sigma_u \leftarrow 1\pi_g$ electronic transition at 234 nm. Different intermediate excited states of atomic fluorine are observed between 126500 and 128500 cm^{-1} in a (3 + 1) ionisation process. Although the initially excited $A^1\Pi_u$ state exclusively correlates to electronic $^2P_{3/2}$ ground state atoms, the fragmentation also generates excited $^2P_{1/2}$ spin–orbit state atoms. The non-adiabaticity is facilitated by the smallness of the spin–orbit splitting $E_\Omega(F) = 404.1$ cm^{-1}. Both time-of-flight and Doppler linewidth measurements agree with the calculated photofragments recoil velocity.

1. Introduction

The state- and energy-resolved detection of nascent fluorine atoms is a major goal in understanding the dynamics of chemical processes involving these atoms. In contrast to other halogen atoms, the observation of atomic fluorine is extremely difficult because high-energy photons are required for resonant excitation. The first resonance transition occurs at 95.5 nm in the far vacuum ultraviolet (VUV) spectral region, well below the LiF window cutoff at 106 nm. Therefore, one-photon excitation not only requires the generation of VUV light but also requires experiments to be performed in windowless reactors. Two-photon excitation seems to be even less promising because it requires the simultaneous absorption of two photons below 200 nm which can only be generated with large technical effort and only at low pulse energies. Therefore, it is not surprising that only a few experiments report the detection and spectroscopy of atomic fluorine [1–10].

Diebold et al. were the first to use a secondary chemical reaction, $F + SM \rightarrow SMF^+ + e$, to indirectly detect the fluorine atom as a primary product of a photodissociation process [1]. Similarly, Sorokin and Chichinin converted primary atomic fluorine into chlorine atoms via the reaction $F + Cl_2 \rightarrow Cl + FCl$ [2]. Clyne and Nip [3] and Sasaki et al. [4–7]

* Corresponding author. Fax: +49 531 391 5832; e-mail: k.gericke@tu.bs.de

0009-2614/99/$ - see front matter
PII: S0009-2614(99)00393-0

applied atomic resonance spectrometry in the far VUV to monitor the $3s^2P_J \leftarrow 2p^5\,^2P_J$ transitions. Stanton and Kolb [8] and Loge et al. [9] used a diode laser to directly observe the spin–orbit splitting $2p^5\,^2P_{1/2}-^2P_{3/2}$.

A certain breakthrough in the state-selective detection of fluorine atoms was achieved by Bischel and Jusinski [10], who reported the observation of resonantly enhanced multi-photon ionisation (REMPI) of this halogen atom, where three photons at 286 nm were required to reach the $3s^2P_J$ resonant intermediates. Since the ionisation limit [11] occurs at 140524.5 cm^{-1}, two additional photons are necessary to ionise the atom. Because the transition probability is very low, to reach the ionisation continuum very high pulse energies (15–20 mJ) at 286 nm had to be applied to obtain an ionisation signal.

The aim of the present work is twofold. First, a (3 + 1)-REMPI technique is introduced to demonstrate the state-selective detection of ^2P_J fluorine atoms where significantly less than 1 mJ pulse energy in a convenient wavelength domain is required to resolve the recoil velocity distribution in a TOF experiment. Second, this analysis technique is applied to study the photodissociation dynamics of F_2:

$$F_2 + h\nu(234\,\mathrm{nm}) \rightarrow 2F\left(^2P_J\right). \qquad (1)$$

The ground state of molecular fluorine exhibits a $X\,^1\Sigma_g^+(3\sigma_g^2\,1\pi_u^4\,1\pi_g^4)$ valence electron configuration. Potential energy curves have been calculated by Cartwright and Hay using modest-sized configuration-interaction calculations [12]. Promoting one π_g electron to the anti-bonding $3\sigma_u$ molecular orbital forms the repulsive $A\,^1\Pi_u$ $(3\sigma_g^2\,1\pi_u^4\,1\pi_g^3\,3\sigma_u)$ state giving rise to the first continuous absorption band centred at about 35000 cm^{-1} (280 nm) [13]. The absorption is blue-shifted with respect to the heavier halogens, and its cross-section is one order of magnitude lower than for Cl_2, the difference to Br_2 and I_2 being even stronger [13]. In contrast to the higher diatomic halogen molecules no contribution of the $a\,^3\Pi_u$ state, which can also be formed by $\pi_g^3\,\sigma_u$ electrons, was observed at longer absorption wavelengths. The $A\,^1\Pi_u$ as well as the $X\,^1\Sigma_g^+$ states (and also the $a\,^3\Pi_u$ state) correlate with fluorine atoms both in their ground state ^2P_J fine-structure manifold.

At 234 nm this simple dissociation proceeds exclusively via the repulsive $A\,^1\Pi_u$ potential energy surface and is of interest for two reasons.

First, it is significantly restricted due to conservation laws. Therefore, the observed recoil velocity v of F atoms can be compared to the calculated one which, in the case of ground state fluorine, is simply given by $v = \sqrt{E_{av}/m}$, where E_{av} is the available energy and m the mass of the F atom.

Second, for the chlorine molecule, it has been found that the dissociation proceeds totally adiabatically, cleanly producing ground state $^2P_{3/2}$ chlorine atoms only [14,15]. The state-selective detection allows the investigation of the adiabaticity of reaction (1), which can be expected to be less than for the other halogens due to the smallness of the spin–orbit interaction $E_\Omega = 404.1$ cm^{-1} of fluorine [16], giving rise to the production of both $^2P_{3/2}$ and $^2P_{1/2}$ spin–orbit state fluorine atoms.

2. Experimental

A detailed description of the experimental arrangement has been given elsewhere [17]. It consists of a home-built single-field time-of-flight (TOF) spectrometer with a ratio of the acceleration region s to the drift region d of 1:2 at a total length of $3s = 57$ cm. The spectrometer was evacuated to a base pressure of 10^{-4} Pa (10^{-6} mbar) by a 360 ls^{-1} turbo molecular pump (Leybold Turbovac 360 CSV) and two 500 ls^{-1} oil diffusion pumps (Leybold Baur 1). A mixture of 5% fluorine in helium (Linde AG) was filled into a glass vessel prior to each experimental run without further purification and fed into the spectrometer via a supersonic jet, generated in an inductively driven pulsed nozzle (General Valve Series 9) with a diameter of 0.5 mm. The valve was operated at a stagnation pressure of typically 8×10^4 Pa (800 mbar) and a pulse duration of 250 μs, resulting in an operational background pressure of less than 10^{-3} Pa (10^{-5} mbar) at a repetition rate of 5 Hz.

Simultaneous dissociation of fluorine and state-selective detection of F atoms was performed using an Nd:YAG laser pumped dye laser (Coherent Infinity/Lambda Physik Scanmate). The dye laser system

was operated with Coumarin-47 at a repetition rate of 5 Hz. Its output was frequency doubled by a BBO crystal, and the wavelength was scanned utilising an auto-tracker unit (Radiant Dyes Scantrack). An energy of typically 150 μJ per pulse was focused into the interaction regime inside the spectrometer by an 80 mm lens. The laser beam intersected the molecular beam at an angle of 45°, while the spectrometer formed an angle of 90° with both the laser and the molecular beam axes. The electric field vector of the linearly polarised laser light was oriented perpendicular with respect to the spectrometer axis. Immediately after each measurement the background signal was monitored with the laser delayed with respect to the gas pulse under otherwise identical conditions and subtracted from the previously obtained TOF profile. Atomic fluorine was resonantly ionised by a (3 + 1)-REMPI scheme, employing the $3d\,^2D_J \rightarrow 2p\,^2P_J^0$ and $3d\,^2P_J \rightarrow 2p\,^2P_J^0$ transitions between 233 and 235 nm both for ground state and for excited spin–orbit state atoms as resonance enhanced steps. Ions were detected by a double stage multi-channel plate assembly (Comstock/Galileo) with an active diameter of 40 mm.

In the acceleration mode, the ions are accelerated by a static electric field of typically 5000 V/m in the acceleration region and detected after passing the drift tube. In the acceleration region the ions are mass selected, and the velocity component v_x along the spectrometer axis is monitored via the mass peak broadening. A linear relationship between the velocity component v_x and the deviation Δt from the centre t_0 of the TOF profile holds for the spectrometer geometry:

$$\Delta t = \frac{8t_0^2}{s} v_x , \qquad (2)$$

where experimental parameters like the acceleration voltage, the ion mass, and the ion charge are contained in the (experimentally observable) quantity t_0. Since the velocity component v_x is perpendicular to the velocity of the molecular beam, no laboratory to centre-of-mass transformation has to be performed. The ion signal is monitored by a digital oscilloscope (LeCroy 9450).

The Doppler mode employs strong acceleration fields of the order of 10^4 V/m in order to assure the arrival of all ions that are generated in one laser pulse at the particle detector. This mode serves for the determination of quantum state populations. Although the Doppler broadening of the spectral lines has not been used for obtaining kinetic energy distributions from the line shape due to the much lower accuracy as compared to the evaluation of the TOF data, it is a most welcome tool for checking the correctness of the kinetic energy distributions, derived from the TOF measurements, by an independent method.

3. Results and discussion

The origin of all observed transitions can exclusively be attributed to fluorine atoms in the $^2P_{3/2}$ ground state or in the $^2P_{1/2}$ excited spin–orbit state. The intermediate resonances in the (3 + 1)-REMPI process are either formed by $2p^4\,4s$ electrons giving rise to $^2P_{1/2}$ and $^2P_{3/2}$ states (spectrum around 237 nm) or by $2p^4\,3d$ electrons giving rise to $^2D_{3/2}$, $^2D_{5/2}$ and $^2P_{1/2}$, $^2P_{3/2}$ terms (spectrum between 233 and 235 nm). As an example, Fig. 1 shows the spectrum for $2p^4\,3d \leftarrow 2p^5$ electron promotion.

^2F and ^2G terms can also be formed by p^4d electrons, but are outside of the dye tuning range. All assigned transitions of Fig. 1 agree with published one-photon excitation energies [11] within 1 cm^{-1} accuracy, considering the three-photon character of the present experiment. Fig. 2 shows the energy level diagram and the induced transitions.

At excitation wavelengths between 233 and 237 nm, only the repulsive $A\,^1\Pi_u$ state can be accessed. Although the absorption cross-section of $\sigma(234\ \text{nm}) \cong 10^{-20}$ cm^2 is fairly small [13] and a pulse energy of only 150 μJ has been used, the $A\,^1\Pi_u \leftarrow X\,^1\Sigma_g^+$ transition is almost saturated due to tight focussing conditions (80 mm focal length).

The $^1\Pi_g$ state of F_2 which can be reached by a $3\sigma_u \leftarrow 1\pi_u$ transition is too high in energy to be excited by a one-photon absorption. Other excited states formed by either valence or Rydberg orbitals need even higher excitation energies. In principle, multi-photon excitation and subsequent fragmentation could also give rise to fluorine atoms. However, then the products would be formed with significantly

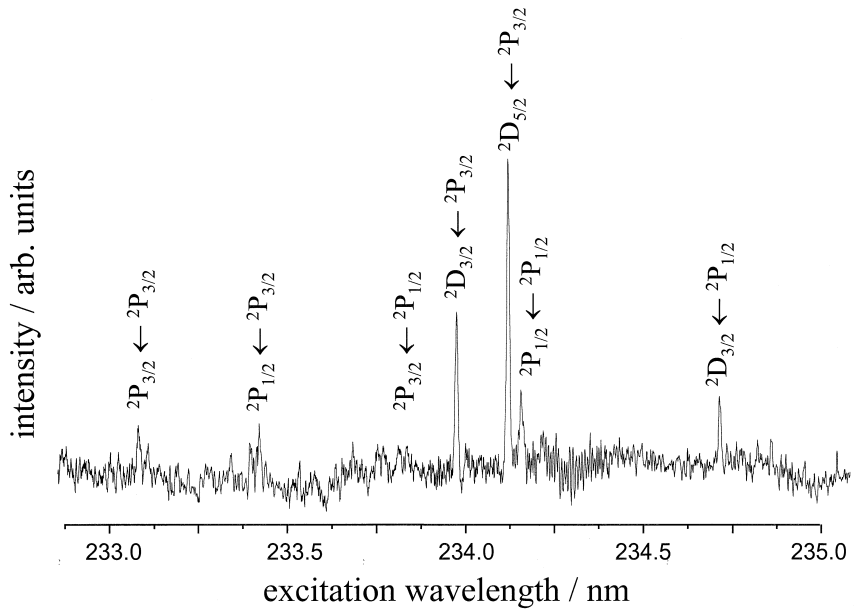

Fig. 1. Spectrum of the $3d\,^2D_J \leftarrow 2p\,^2P^0_J$ and $3d\,^2P_J \leftarrow 2p\,^2P^0_J$ three-photon resonant transitions between 233 and 235 nm for ground state and for excited spin–orbit state fluorine atoms.

higher recoil velocities than when originating from the $A\,^1\Pi_u$ state. Since this was not observed, we conclude that only the dissociation dynamics of

$$F_2\left(^1\Pi_u\right) \rightarrow F\left(^2P_J\right) + F\left(^2P_{J'}\right) \qquad (3)$$

is investigated in the present experiment.

The correlation between the electronic molecular states of F_2 and the fine-structure states of the separated fluorine atoms in the adiabatic limit can be obtained following the approach of Singer et al. [18] and of Matsumi and Kawasaki [19]. The total angular momentum in the dissociating molecule is expressed according to the coupling scheme of Hund's case (c), since in the course of the dissociation the interaction between L and S becomes stronger than the interaction with the internuclear axis [20].

In Hund's case (a) notation, the three lowest electronic states of molecular fluorine are the $X\,^1\Sigma_g^+(3\sigma_g^2\,1\pi_u^4\,1\pi_g^4)$ ground state and the $A\,^1\Pi_u$ and the $a\,^3\Pi_u(3\sigma_g^2\,1\pi_u^4\,1\pi_g^3\,3\sigma_u)$ excited states. In Hund's case (c) notation, the orbital and spin angular momentum components Λ and Σ cease to be good quantum numbers and only the total angular momentum component $\Omega = |\Lambda - \Sigma|, \ldots, \Lambda + \Sigma$ and the symmetry properties of the electronic wavefunction can be used to characterise the electronic state. Two fluorine atoms in the $^2P_{3/2}$ ground state form 16

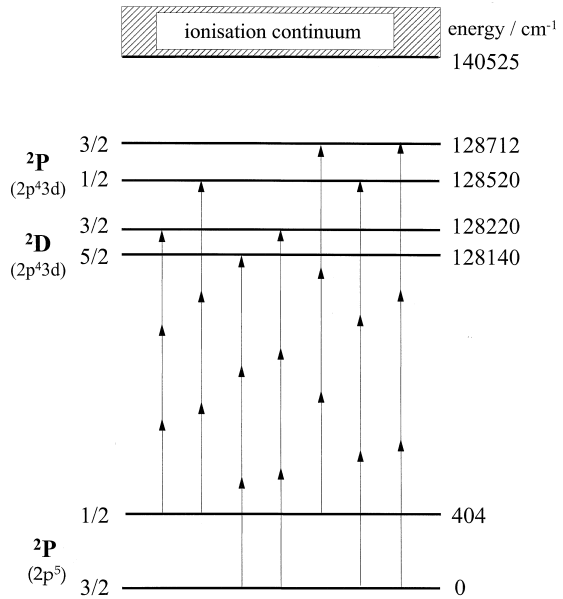

Fig. 2. Energy level scheme of the atomic states giving rise to the spectrum shown in Fig. 1. Energy levels are not to scale for increased clarity.

Table 1
Correlation between F_2 molecular states in Hund's case (c) notation and (J, J') eigenstate pairs of the separated F atoms, where $\Omega = |M_J + M'_J|$

J, J'	$\Omega = 0$	$\Omega = 1$	$\Omega = 2$	$\Omega = 3$
3/2, 3/2	$0_g^+, 0_g^+, 0_u^-, 0_u^-$	$1_g, 1_u, 1_u$	$2_g, 2_u$	3_u
3/2, 1/2 1/2, 3/2	$0_g^+, 0_g^-, 0_u^+, 0_u^-$	$1_g, 1_g, 1_u, 1_u$	$2_g, 2_u$	
1/2, 1/2	$0_g^+, 0_u^-$	1_u	1_u	

Data are taken from Ref. [21].

states with $0 \leqslant \Omega \leqslant 3$, one atom in the $^2P_{3/2}$ and one in the $^2P_{1/2}$ state form another 16 states with $0 \leqslant \Omega \leqslant 2$, and two atoms in the $^2P_{1/2}$ state form four states with $0 \leqslant \Omega \leqslant 1$ [21], which are explicitly listed in Table 1. Accordingly, the $X\,^1\Sigma_g^+(0_g^+)$ state and the $A\,^1\Pi_u(1_u)$ state correlate with the respective 0_g^+ and 1_u states formed by two $^2P_{3/2}$ ground state atoms. This also holds for the $a\,^3\Pi(2_u, 1_u, 0_u^-)$ states. Only the $a^3\Pi(0_u^+)$ state correlates with the 0_u^+ state formed by one $^2P_{3/2}$ ground state atom and by one $^2P_{1/2}$ excited state atom.

Fig. 1, however, proves the existence of transitions originating from both the $^2P_{3/2}$ ground state and the $^2P_{1/2}$ excited state. Thus, both spin–orbit states are populated in the dissociation of F_2 from the $A\,^1\Pi_u$ state, and the process cannot properly be described by the adiabatic limit.

In the diabatic limit, the separated atom states are coupled together in the exit channel, provided Ω and the symmetry properties are conserved. If we number the six atomic states J, M_J by $i = 1$–6, then according to Table 2 the unnormalised joint probability matrix for realising states with $\Omega = 1$ becomes:

$$P(i,j) = \begin{pmatrix} 0 & 0 & 1 & 0 & 0 & 1 \\ 0 & 1 & 0 & 1 & 1 & 0 \\ 1 & 0 & 1 & 0 & 0 & 1 \\ 0 & 1 & 0 & 0 & 1 & 0 \\ 0 & 1 & 0 & 1 & 1 & 0 \\ 1 & 0 & 1 & 0 & 0 & 1 \end{pmatrix} \tag{4}$$

Summation over columns (or rows) gives:

$$P(i) = (2, 3, 3, 3, 2, 3, 3) \tag{5}$$

corresponding to 10 $P_{3/2}$ states ($i = 1$–4), six of which are ungerade and four are gerade, and six $P_{1/2}$ states ($i = 5,6$), four of which are ungerade and two are gerade. Therefore, accounting for states of ungerade symmetry with $\Omega = 1$ only, a diabatic branching ratio of $P(^2P_{3/2})/P(^2P_{1/2}) = 3{:}2$ is expected.

Without a knowledge of the three-photon transition probabilities, we can only perform a qualitative analysis of the spectrum in Fig. 1. The four strongest transitions are $^2D_{5/2} \leftarrow {}^2P_{3/2}$, $^2D_{3/2} \leftarrow {}^2P_{3/2}$, $^2P_{1/2} \leftarrow {}^2P_{1/2}$, $^2D_{3/2} \leftarrow {}^2P_{1/2}$. Clearly, with the $^2P_{3/2}$ state as the origin, signal intensities are higher by a factor of 2 to 3, compared to the transitions originating from the $^2P_{1/2}$ state. Therefore, we do not expect a dramatic deviation from a statistical distribution for the two spin–orbit states. However, it should be mentioned that the degree of adiabaticity, and thus the spin–orbit state population, may vary with the

Table 2
Joint reaction probabilities for $F(J, M_J) + F(J', M'_J)$ partner products under the provision that $\Omega = 1$ be maintained

		J, M_J					
i	J', M'_J	3/2, 3/2	3/2, 1/2	3/2, −1/2	3/2, −3/2	1/2, 1/2	1/2, −1/2
1	3/2, 3/2	0	0	1/16	0	0	1/16
2	3/2, 1/2	0	1/16	0	1/16	1/16	0
3	3/2, −1/2	1/16	0	1/16	0	0	1/16
4	3/2, −3/2	0	1/16	0	0	1/16	0
5	1/2, 1/2	0	1/16	0	1/16	1/16	0
6	1/2, −1/2	1/16	0	1/16	0	0	1/16

5/8 of all products are found in the $^2P_{3/2}$ state and the remaining 3/8 are generated in the excited $^2P_{1/2}$ state, if only statistically processes govern the dissociation process.

dissociation wavelength. Similar effects were observed in the photodissociation of Cl_2 [15].

TOF profiles of ejected fluorine atoms have been measured at different acceleration voltages using the $^2D_{5/2}(3d) \leftarrow {}^2P_{3/2}$ and the $^2D_{3/2}(4s) \leftarrow {}^2P_{3/2}$ resonant transitions. As an example the TOF profile of the $^2D_{5/2} \leftarrow {}^2P_{3/2}$ transition at a 234.1 nm excitation wavelength is shown in Fig. 3. Fragment fly-out is significant due to the relatively low acceleration voltage of 1 kV [22]. Therefore, the signal is small and exhibits a pronounced dip at the profile centre, but the recoil velocity can be accurately determined. From the profile in Fig. 3, we obtain a fragment velocity of (4280 ± 130) ms^{-1}. Since the F_2 photodissociation results in two fluorine atoms, the recoil velocities v for each spin–orbit state pair are single-valued and determined by the conservation of energy and linear momentum: $v = \sqrt{E_{av}/m}$. Here, the available energy E_{av} is determined by the photon energy $h\nu$, the dissociation energy $D_0(F_2) = 12920$ cm^{-1} [23], and the internal product energy E_I:

$$E_{av} = h\nu - D_0 - E_I . \quad (6)$$

The F_2 parent molecule initial energy in the molecular beam amounts to less than 10 cm^{-1} and can therefore be neglected. For the $^2D_{5/2} \leftarrow {}^2P_{3/2}$ transition, the internal energy of the probed product is zero while the partner fragment might be generated in either the ground state ($E_I = 0$) or the excited spin–orbit state ($E_I = E_\Omega$). However, the energy difference of 404.1 cm^{-1} (see Fig. 2) does not significantly influence the recoil velocity: for a $^2P_{3/2} + {}^2P_{3/2}$ ($^2P_{3/2} + {}^2P_{1/2}$) pair correlation one calculates product velocities of 4330 ms^{-1} (4300 ms^{-1}), which is in excellent agreement with the experimental value. We would like to mention that a two-photon absorption of F_2 would result in recoil velocities of 6700 ms^{-1}.

Although the velocity resolution of ca. 2.5% [22] is not sufficient to experimentally determine from the observed TOF lineshapes the normalised joint reaction probability $P_{1u}(J, J')$ for producing a (J, J') F atom pair originating from a 1_u state, we like to note that, assuming a statistical distribution, from the state correlation of Table 1 one obtains:

$$P_{1u}(J, J') = \frac{1}{10}\begin{pmatrix} 4 & 2 \\ 2 & 2 \end{pmatrix}. \quad (7)$$

The probability for $(3/2, 3/2)$ pair formation is equal to the probability for $(3/2, 1/2)$ and $(1/2, 3/2)$

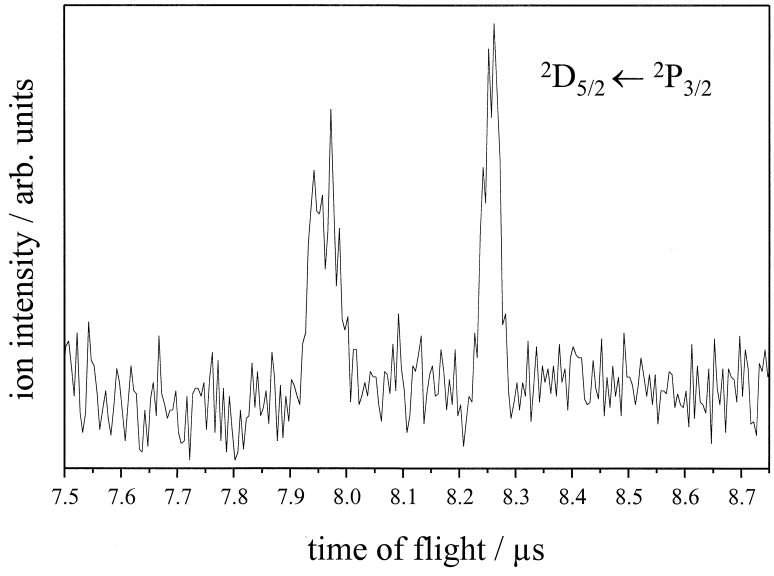

Fig. 3. TOF profile of ground state fluorine obtained in the acceleration mode. The two clearly separated peaks belong to one velocity broadened mass peak ($m = 19$) and correspond to forward and backward flying atomic fragments. The wing separation is a measure of fragment velocity. The peak center is depleted due to ion fly-out.

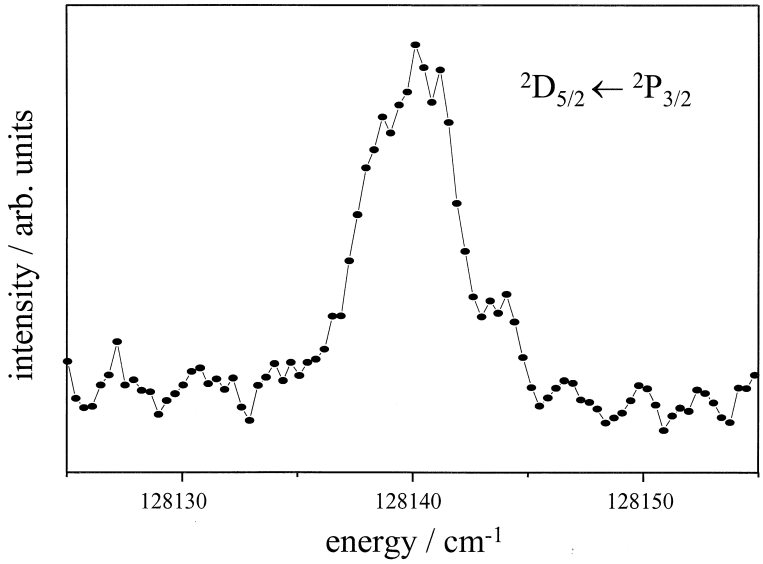

Fig. 4. Doppler profile for the same transition as shown in Fig. 3. The kinetic energy obtained from the width of the Doppler profile agrees well with the value obtained from the analysis of the acceleration TOF profile of Fig. 3.

pair formation: $P_{1u}(3/2, 3/2) = P_{1u}(3/2, 1/2) + P_{1u}(1/2, 3/2) = 0.4$. Thus, an equal contribution of $^2P_{3/2}$ and $^2P_{1/2}$ partner products to an observed $^2P_{3/2}$ state TOF profile can be expected for a statistical decay.

A less accurate determination of the recoil velocities can be obtained from a measurement of the Doppler linewidth. Fig. 4 shows the Doppler profile of the $^2D_{5/2} \leftarrow {}^2P_{3/2}$ line at a transition energy of 128120 cm^{-1}. Here, the dye laser was tuned around 234 nm, and a sufficiently high acceleration voltage was applied in order to collect all F^+ ions generated in the $(3 + 1)$-REMPI process. For the calculated recoil velocity of 4330 ms^{-1}, we expect a Doppler width of 3.8 cm^{-1} (FWHM) considering the laser linewidth. The experimental value of 4.4 cm^{-1} is in fair agreement with the calculation. Since the detection process is highly nonlinear, profile measurements are very sensitive to laser fluctuations and no better agreement than 10% can be expected.

In summary, nascent fluorine atoms can be detected in a state- and velocity-resolved manner. The required pulse energies slightly above 100 μJ are easily obtainable from laser systems now available, and future elucidation of the dynamics of photodissociation and reactive processes involving fluorine atoms has become possible. A first demonstration is given by the photodissociation of $F_2(^1\Sigma_g^+) + h\nu \rightarrow F_2(^1\Pi_u) \rightarrow 2F(^2P_J)$ where both spin–orbit states can easily be resolved and the velocity of the atomic fluorine product can be detected by both TOF and Doppler profile measurements.

Acknowledgements

The authors gratefully acknowledge financial support of the Deutsche Forschungsgemeinschaft and the Japan Society for the Promotion of Science. MK thanks NEDO for financial support of this project. MR thanks the Fonds der Chemischen Industrie for fellowship support.

References

[1] G.J. Diebold, F. Engelke, D.M. Lubman, J.C. Whitehead, R.N. Zare, J. Chem. Phys. 67 (1977) 5407.
[2] V.I. Sorokin, A.I. Chichinin, Chem. Phys. Lett. 280 (1997) 141.
[3] M.A.A. Clyne, W.S. Nip, J. Chem. Soc. Faraday Trans. II 73 (1977) 1308.
[4] K. Sasaki, Y. Kawai, K. Kadota, Rev. Sci. Instrum. 70 (1999) 76.

[5] K. Sasaki, Y. Kawai, C. Suzuki, K. Kadota, J. Appl. Phys. 83 (1998) 7482.
[6] K. Sasaki, Y. Kawai, K. Kadota, Appl. Phys. Lett. 70 (1997) 1375.
[7] K. Sasaki, Y. Kawai, C. Suzuki, K. Kadota, J. Appl. Phys. 82 (1997) 5938.
[8] A.C. Stanton, C.E. Kolb, J. Chem. Phys. 72 (1980) 6637.
[9] G.W. Loge, N. Nereson, H.A. Fry, Appl. Opt. 33 (1994) 3161.
[10] W.K. Bischel, E. Jusinski, Chem. Phys. Lett. 120 (1985) 337.
[11] S. Bashkin, J.O. Stoner, Jr., Atomic Energy Levels and Grotrian Diagrams, vol. 1, North-Holland, Amsterdam, 1975, p. 213.
[12] D.C. Cartwright, P.J. Hay, Chem. Phys. 114 (1987) 305.
[13] R.K. Steunenberg, R.C. Vogel, J. Am. Chem. Soc. 78 (1956) 901.
[14] L. Li, R.J. Lipert, J. Lobue, W.A. Chupka, S.D. Colson, Chem. Phys. Lett. 151 (1988) 335.
[15] Y. Matsumi, K. Tonokura, M. Kawasaki, J. Chem. Phys. 97 (1992) 1065.
[16] NIST-JANAF Thermochemical Tables, M.W. Chase, Jr. (Ed.), J. Phys. Chem. Ref. Data, Monograph 9, 1998, p. 1051.
[17] T. Haas, C. Maul, K.-H. Gericke, F.J. Comes, Chem. Phys. Lett. 202 (1993) 108.
[18] S.J. Singer, K.F. Freed, Y.B. Band, Adv. Chem. Phys. 61 (1985) 1.
[19] Y. Matsumi, M. Kawasaki, J. Chem. Phys. 93 (1990) 2481.
[20] G. Herzberg, Molecular Spectra and Molecular Structure vol. I, Spectra of Diatomic Molecules, Van Nostrand Reinhold, New York, 1950, p. 225 and p. 244.
[21] G. Herzberg, Molecular Spectra and Molecular Structure vol. I, Spectra of Diatomic Molecules, Van Nostrand Reinhold, New York, 1950, pp. 319–322.
[22] C. Maul, T. Haas, K.-H. Gericke, F.J. Comes, J. Chem. Phys. 102 (1995) 3238.
[23] G. Huber, G. Herzberg, Molecular Spectra and Molecular Structure IV, Constants of Diatomic Molecules, Van Nostrand Reinhold, New York, 1979, p. 214.